Nanoscale

PAPER

View Article Online
View Journal | View Issue

Cite this: *Nanoscale*, 2024, **16**, 9819

Exceptional behavior of a high-temperature superconductor in proximity to a ferromagnet in a bilayer film, $La_{0.67}Sr_{0.33}MnO_3/YBa_2Cu_3O_7$

Ankita Singh, Sawani Datta, Ram Prakash Pandeya, Srinivas C. Kandukuri, Rudheer Bapat, Jayesh Parmar and Kalobaran Maiti *

We studied the electronic properties of a high-temperature superconductor in proximity to a ferromagnetic material in a bilayer film of $La_{0.67}Sr_{0.33}MnO_3$ (LSMO)/$YBa_2Cu_3O_7$ (YBCO). High-quality single-crystalline films of YBCO and LSMO/YBCO were grown epitaxially on an $SrTiO_3$ (001) surface. Magnetization data of the LSMO/YBCO bilayer exhibit ferromagnetic transition at about 255 K, which is much smaller than the Curie temperature of bulk LSMO. Experimental data show the emergence of magnetic anisotropy with cooling, which becomes significantly stronger in the superconducting phase. The onset temperature of diamagnetism is observed at 86 K in the YBCO sample for the out-of-plane magnetization and at 89 K in the in-plane data. Interestingly, the diamagnetism sets in at about 86 K for both magnetization directions in the LSMO/YBCO film despite the presence of the ferromagnetic LSMO layer underneath. Ba 4d and Y 3d core-level spectra show different surface and bulk electronic structures. Surface contribution is reduced significantly in the LSMO/YBCO sample, suggesting enhanced bulk-like behavior due to an enhancement of electron density near the surface arising from charge transfer across the interface. These results reveal an outstanding platform for on-demand tuning of properties without affecting the superconductivity of the system for the exploration of fundamental science and applications in advanced technology.

Received 28th December 2023,
Accepted 22nd April 2024

DOI: 10.1039/d3nr06636c

rsc.li/nanoscale

1. Introduction

Superconductivity and magnetism are two mutually exclusive phenomena as the zero resistance condition can completely block the penetration of magnetic lines of force through materials as demonstrated by the Meissner effect. Application of a magnetic field destroys superconductivity beyond a critical field and the penetration of lines of force, called vortices, is studied in the intermediate field regime extensively. While some materials show coexisting antiferromagnetic order and superconductivity,[1,2] it is not clear if both these behaviors occupy the same phase space. In general, it is difficult to achieve both kinds of behavior coexisting in the same bulk system and attempts have been made to prepare materials in the form of heterostructures of thin films having competing interactions.[3–6] The antagonistic behavior of the materials may lead to exotic scenarios as the superconductivity tends to expel the magnetic lines of force limiting them to within the magnetic film and/or the spin-polarized quasiparticle injection occurs across the interface.[7]

In a typical superconductor, electrons of opposite momenta form Cooper pairs, wherein ferromagnetic compounds, exchange interaction tends to align magnetic spins in the direction of the applied magnetic field. Thus, the ferromagnetic layer influences the critical current and vortex pinning strength in the superconducting layer, while the Cooper pairs in the superconducting layer may renormalize the magnetic exchange interactions within the ferromagnetic layer. To study this scenario, bilayer films of magnetic and superconducting materials have been studied extensively in the literature.[8–11] $La_{0.67}Sr_{0.33}MnO_3$ (LSMO) and $YBa_2Cu_3O_7$ (YBCO) are found to be good candidate materials for epitaxial growth with sharp interfaces due to their similar *a*/*b* lattice parameters. Various studies show exotic phenomena such as domain wall superconductivity,[12] triplet superconductivity,[13] change in vortex behavior,[14,15] *etc.* In a study by H.-Ye Wu *et al.*[16] on superconducting/ferromagnetic multilayers, an enhancement of critical current density is reported in the low field regime, exhibiting the presence of a strong vortex pinning effect due to the presence of spin–vortex interaction. In other studies[17,18] of LSMO/YBCO superlattices, the presence of anisotropy in LSMO layers and an exchange biasing effect are also observed.[17] The charge carrier density significantly influences the properties of LSMO[19–22] and YBCO.[23] Thus, the injection of spins from the ferromagnetic layer to the super-

Department of Condensed Matter Physics and Materials Science, Tata Institute of Fundamental Research, Homi Bhabha Road, Colaba, Mumbai-400005, India. E-mail: kbmaiti@tifr.res.in

conducting one in the heterostructure will break the time reversal symmetry of the Cooper pairs due to excess magnetic moments and quasiparticle redistribution,[24] leading to a suppression of superconducting transition temperature, T_c. Evidently, the properties of heterostructures involving magnetic and superconducting layers are an interesting area with emerging exoticism arising from their interaction across the interface, which is an unknown paradigm. In the present work, we study the growth, and structural and magnetic properties of an LSMO/YBCO bilayer film. Our results reveal exceptional properties of the YBCO layer in the presence of the ferromagnetic layer underneath and evidence of charge transfer across the interface.

2. Experimental details

YBCO and LSMO films were grown on an $SrTiO_3$ (001) surface using a custom-built ultra-high vacuum (UHV) pulsed laser deposition (PLD) system equipped with a KrF excimer laser (λ = 248 nm) set at 5 Hz frequency. We used commercially available targets ($La_{0.67}Sr_{0.33}MnO_3$ and $YBa_2Cu_3O_7$) and the target to substrate distance was maintained at 5 cm. LSMO layers were grown with laser fluence of 1.5 J cm^{-2}, substrate temperature of 750 °C and oxygen partial pressure of 300 mTorr. The growth parameters for YBCO were set at 1.8 J cm^{-2}, 850 °C and 400 mTorr, respectively. The thickness of the films was monitored by the number of laser pulses used for deposition; 3000 shots for the LSMO layer (~100 nm) and 21 000 shots for the YBCO layer (~500 nm) in all cases. The films were *in situ* annealed for 1.5 hours under 500 Torr oxygen pressure in the deposition chamber and then slowly cooled down to room temperature.

The crystallinity and epitaxial quality of the films were studied by X-ray diffraction (XRD) measurements. For the structural properties of the films, we used the $\theta/2\theta$ scan mode of a Rigaku diffractometer. Pole figure data were recorded for the tilt angle, φ (0°–90°), and the azimuthal angle, ψ (0°–360°). Reciprocal space mapping was carried out for the YBCO (119) Bragg peak. Magnetic measurements were performed using a SQUID magnetometer (MPMS XL Evercool, Quantum Design).

In order to study the surface quality of the films, we captured scanning electron microscopy (SEM) images using a Zeiss ULTRA plus field emission SEM (FESEM) system. The single crystallinity and quality of the interface were assessed using a high-resolution aberration-corrected scanning transmission electron microscope from FEI TITAN operating at 300 kV. Analysis of the electronic structure of the thin film was carried out by means of X-ray photoelectron spectroscopy (XPS) using an R4000 Scienta analyzer and a monochromatic Al Kα source at an energy resolution of 0.4 eV.

3. Results and discussion

YBCO forms an orthorhombic structure having lattice parameters a = 3.82 Å, b = 3.89 Å, and c = 11.68 Å.[25] These a and b values are comparable to the lattice parameter of the STO substrate (a = 3.905 Å) and the pseudocubic lattice parameter of LSMO (a = 3.87 Å),[9] which is good for the high-quality epitaxial growth of both these layers on the STO substrate. We analysed the crystal structure of the films grown employing X-ray diffraction techniques. A typical XRD scan of the bilayer film is shown in Fig. 1(a). XRD patterns of the target materials are shown in the lower panel of the figure. In the case of the LSMO sample, (00l) is not distinctly visible, presumably due to the use of the target instead of the powdered sample; the structural parameters are similar to earlier reports.[9] The XRD pattern of the YBCO film is consistent with that of the bulk YBCO data, indicating close structural parameters in both cases. No secondary phase is observed for YBCO and LSMO. The XRD data of the bilayer indicate (00l)-oriented growth in all cases, suggesting good single crystallinity of the samples.[26]

In order to investigate the epitaxial quality and orientation of the films further, we performed pole figure measurements for the YBCO (229) reflection of the bilayer film. Since, the (229) reflection of YBCO was not found in the $\theta/2\theta$ scan, we explored the in-plane reflections for these measurements; the YBCO (229) plane appears at α (90° − φ) = 5°. The experimental pole figure data are shown in Fig. 1(b) with the azimuthal angle, ψ, as the circumference axis and α as the radial direction at an expanded scale of 0–5°. The data exhibit four distinct features with the highest intensity at α = 5°, which is consistent with the growth having the (00l) direction as the out-of-plane axis. Reciprocal space mapping (RSM) was performed for the (119) reflection of YBCO, as shown in Fig. 1(c). It is evident that the broadening axis of YBCO makes an angle with the Q_x direction and has an elliptical shape, suggesting the presence of a mosaic structure.[27,28] We calculated the lateral correlation length and microscopic tilts that provide information about the average block size and out-of-plane disorientation, respectively, which results in an elliptical shape. The calculated lateral correlation length and microscopic tilt for YBCO is found to be 187.72 nm and 0.018°, respectively, which demonstrates high-quality epitaxial growth along the (00l) direction. The center of the substrate and the YBCO layer does not lie in the same vertical line, indicating relaxed growth of the YBCO film. The in-plane and out-of-plane lattice parameters are estimated to be 3.92 Å and 11.84 Å, respectively, which are close to the bulk lattice parameters.

FESEM images of the STO/YBCO and STO/LSMO/YBCO samples are shown in Fig. 1(d) and (e), respectively, exhibiting high-quality smooth surfaces of the samples in both cases. The high-resolution TEM image of the cross-section of the STO/LSMO/YBCO sample shown in Fig. 1(f) exhibit well-resolved ordered atom positions with a sharp interface in both cases. The fast Fourier transform (FFT) of the TEM data shown at the right exhibits a high-quality sharp pattern, demonstrating the excellent crystalline quality of the samples.

Magnetization measurements (zero field cooled, ZFC and field cooled, FC) were performed in the temperature range of 2–350 K at magnetic fields of 50 Oe, 100 Oe and 5 kOe. The experimental results are shown in Fig. 2; the data for YBCO

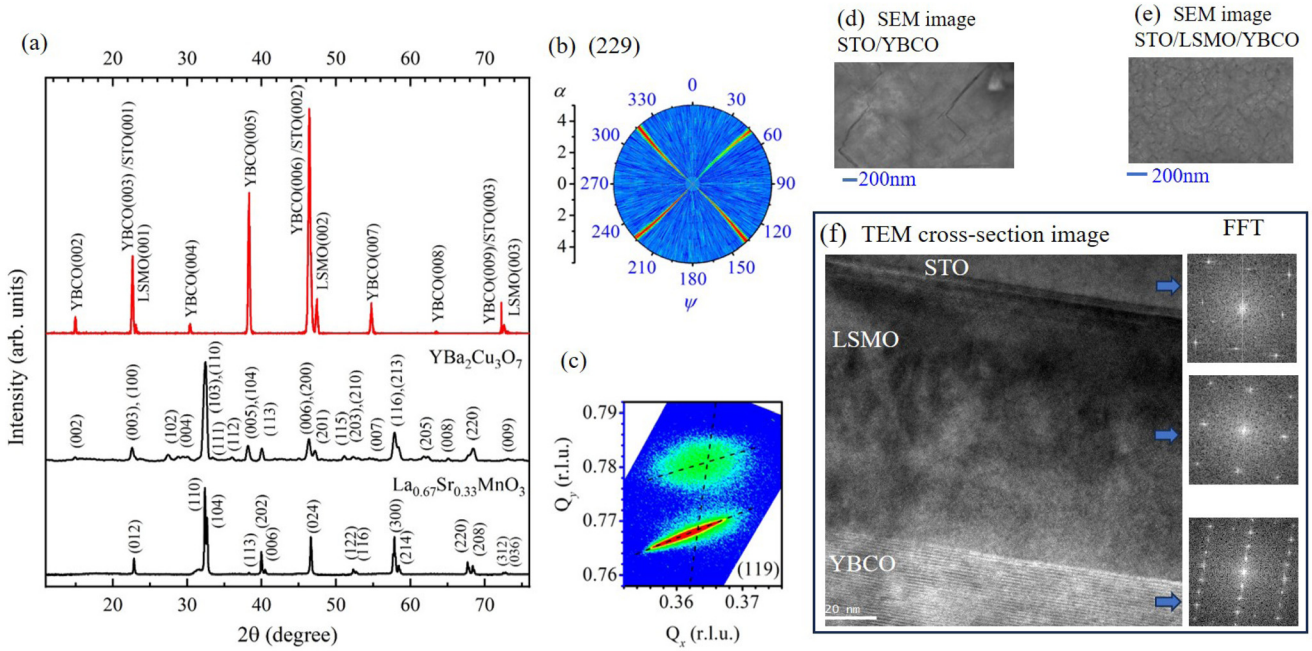

Fig. 1 (a) XRD pattern of the LSMO/YBCO bilayer on an STO substrate. XRD patterns of the target materials (LSMO and YBCO) are shown in the lower panel. (b) Pole figure data for the YBCO (229) line of the LSMO/YBCO sample. (c) Reciprocal space mapping along YBCO (119). (d) FESEM images of the STO/YBCO surface. (e) FESEM image of the STO/LSMO/YBCO surface. (f) High-resolution TEM cross-section image of the STO/LSMO/YBCO film. The images of the right panel are the FFT data exhibiting excellent single crystallinity of the sample in all the layers.

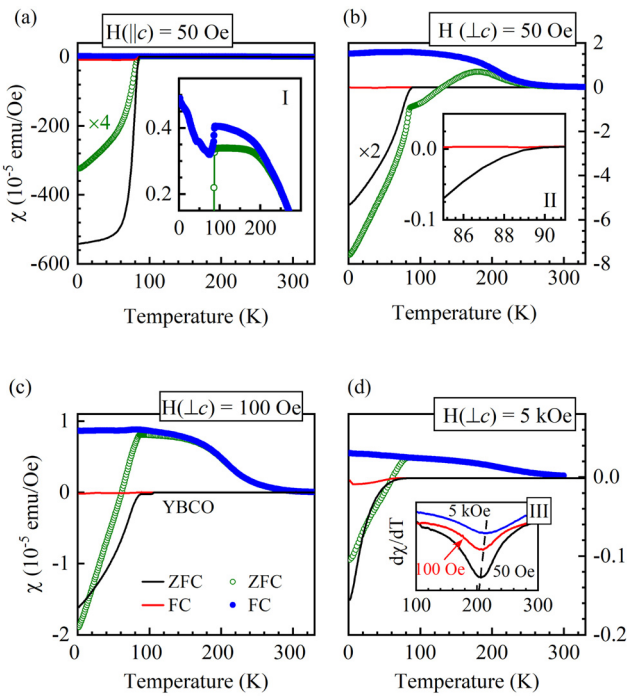

Fig. 2 Magnetization data of LSMO/YBCO (symbols) and YBCO (lines) films at H = 50 Oe: (a) H ||*c*-axis and (b) H ⊥*c*-axis. Inset I: expanded LSMO/YBCO data in (a). Inset II: expanded YBCO data in (b). Magnetization data (*H*⊥*c*-axis) for fields of (c) 100 Oe and (d) 5 kOe. Inset III: derivative of LSMO/YBCO data at 50 Oe, 100 Oe, and 5 kOe ⊥*c*-axes.

and LSMO/YBCO films are represented by lines and symbols, respectively. In Fig. 2(a), we have shown the data collected at 50 Oe magnetic field along the *c*-axis; the data for the LMSO/YBCO sample is multiplied by 4 for clarity. The onset temperature of superconductivity, T_c, is found to be close to 86 K. The magnetization data for the LSMO/YBCO sample exhibit ferromagnetic order at about 255 K, which is significantly smaller than the bulk Curie temperature of 360 K (ref. 29) and the 340–350 K observed in films of thickness 29–40 nm.[30,31] The reasons for the lower Curie temperature in our sample may be related to the structural modification due to slightly different lattice parameters of the substrate and the overlayers, imperfections in the materials,[32,33] and/or transfer of charge carriers between the YBCO and LSMO layers, leading to a differently doped composition.[19–23] A sharp magnetization drop close to 87 K is observed, signifying the onset of superconductivity despite the presence of a ferromagnetic layer underneath. The weaker diamagnetic moment in the LSMO/YBCO case can be attributed to the contributions arising from the ferromagnetic LSMO layer; this is evident in the FC curve shown in inset I, exhibiting a gradual increase in moment with cooling at low temperatures. In LSMO/YBCO systems, suppression of T_c was observed in earlier studies.[10] The absence of such behavior in the present case may be due to the larger thickness of the YBCO layer in our study, suggesting a unique platform to tune the properties of electrons without affecting the superconductivity of the system.

In Fig. 2(b), we have shown the magnetization data for the in-plane field of 50 Oe (⊥*c* direction). The ZFC curve of the

YBCO film shows the onset of superconductivity at a slightly higher temperature (~89 K) with the diamagnetic moments significantly less than the values observed for the out-of-plane case, suggesting that the in-plane magnetic field has a relatively smaller effect on the superconductivity. The data for the bilayer film exhibit a ferromagnetic transition at about 255 K, consistent with the ||*c*-case, although the magnetic moments are significantly larger in this case. Interestingly, transition to the superconducting phase occurs at 86 K in the ZFC data of the LSMO/YBCO sample, as also observed in the out-of-plane case. Curiously, the diamagnetic moment for the in-plane magnetization is found to be larger than that in the pristine case. Moreover, the ZFC curve shows a gradual decrease and becomes negative at a much higher temperature (~130 K).

The magnitude of the diamagnetic signal for out-of-plane magnetization is significantly larger than that for the in-plane case. Another important difference between the in-plane and out-of-plane data is observed in the FC curve, exhibiting a drop in magnetization at T_c for the out-of-plane direction, which then again increases, whereas the in-plane FC curve does not show such features down to the lowest temperature studied. This suggests that diamagnetism has a dominant effect for the out-of-plane magnetization and the magnetic easy axis is along the in-plane field of the LSMO/YBCO bilayer as expected due to shape anisotropy. The slightly smaller superconducting transition temperature, T_c, in LSMO/YBCO relative to YBCO for the in-plane case may be attributed to the following scenarios: (i) a magnetic field due to the ferromagnetic LSMO layer destroys the Cooper pairs and/or superconducting coherence close to the transition although eventually superconductivity sets in at a slightly lower temperature. (ii) Charge transfer across the interface leading to a hole concentration corresponding to a lower T_c.[9] The onset temperature of superconductivity in both samples, LSMO/YBCO and YBCO films, is identical for the out-of-plane field.

In Fig. 2(c) and (d), we have shown the ZFC and FC data of YBCO and LSMO/YBCO films at in-plane magnetic fields of 100 Oe and 5 kOe. In the YBCO film, the higher applied field reduces the diamagnetic susceptibility, χ, manifesting the gradual destruction of the Meissner effect; the bifurcation of FC/ZFC curves occurs at 85 K and 65 K for 100 Oe and 5 kOe, respectively. In the LSMO/YBCO film, χ is positive at higher temperatures. The FC/ZFC curves bifurcate at about 84 K and 76 K for the fields of 100 Oe and 5 kOe, respectively. While the reduction of T_c due to the application of a magnetic field is in line with the expected behavior, curiously, T_c at 5 kOe is higher in the LSMO/YBCO film compared to that in the pristine case. The inset of Fig. 2(d) shows the variation of the first derivative of susceptibility with the temperature in the vicinity of the ferromagnetic Curie temperature. The minima of the first derivative curve appear at 206 K, 210 K and 216 K for 50 Oe, 100 Oe and 5 kOe, respectively, indicating enhancement of the ferromagnetic ordering temperature with the increase in field. Application of a stronger magnetic field usually helps to align the moments better without much effect on the ordering temperature. However, the enhancement of the ordering temperature in this system suggests that the YBCO layer has significant influence on exchange coupling within the LSMO layer even when the material is not superconducting, and thereby changes the magnetic ordering temperature.

Magnetic hysteresis loops of the LSMO/YBCO bilayer measured at 100 K and 200 K are shown in Fig. 3(a) and (b), respectively. The data at 200 K exhibit almost similar behavior with the saturation moment for the out-of-plane direction being slightly larger than the in-plane moment. At 100 K, the results indicate significantly different behavior with the emergence of large magnetic anisotropy at higher fields. While the area inside the loop is small in both cases, the saturation moment is larger in the out-of-plane direction. The in-plane magnetization exhibits faster saturation than the out-of-plane magnetization.

In Fig. 3(c), we have shown the magnetic hysteresis loops at 40 K–70 K for the LSMO/YBCO bilayer for the in-plane fields. The hysteresis loops show complex behavior, exhibiting an interplay between the Meissner currents in the YBCO layer and the ferromagnetic moments in the LSMO layer. While the behavior indicates the presence of diamagnetism, the hysteresis loops exhibit a plateau at higher field, indicating a signature of compensation of the change in magnetic moments due to the field. This suggests a strong proximity effect of the YBCO layer on the magnetism of the LSMO layer involving charge

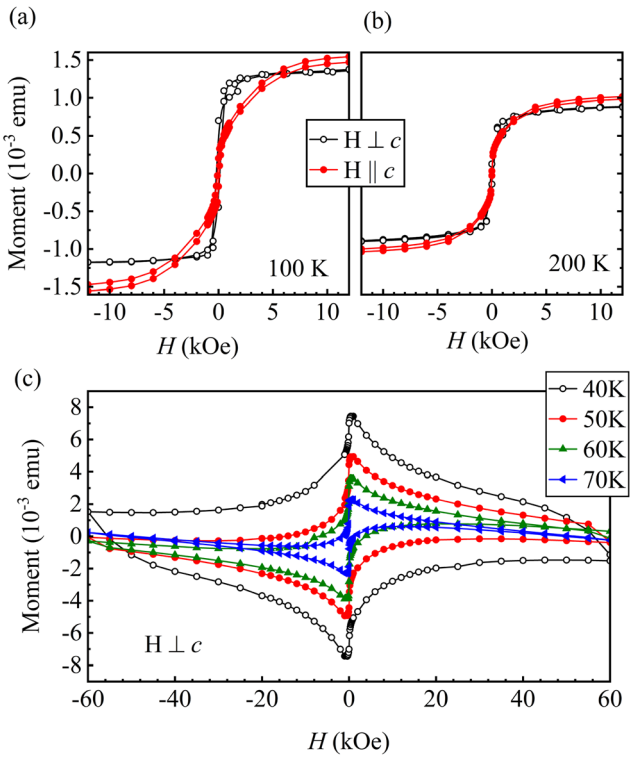

Fig. 3 Magnetization loops of the LSMO/YBCO bilayer for the magnetic field ||*c*-axis (closed circles) and ⊥*c*-axis (open circles) at (a) 100 K and (b) 200 K. (c) Magnetization loops at 40, 50, 60, and 70 K for the field ⊥*c*-axis.

transfer across the interface and the presence of Cooper pairs.[34] From the phase diagram of $La_{1-x}Sr_xMnO_3$,[18] it is known that the material shows an antiferromagnetic phase for the doping level $x > 0.48$. Thus, in the bilayer film, few LSMO layers near the interface have possibly gone into an antiferromagnetic state due to charge transfer.[17,18] While the behavior remains almost similar, the moments are enhanced with the decrease in temperature, suggesting enhanced diamagnetism due to the superconductivity of the YBCO layers.

Magnetic hysteresis loops measured at 2 K are shown in Fig. 4 for the in-plane and out-of-plane magnetization directions. The data for YBCO and LSMO/YBCO are shown by open and closed circles, respectively. For in-plane magnetization, the data shown in Fig. 4(a) exhibit a slightly different magnetic moment for the YBCO and LSMO/YBCO cases. While the YBCO film shows typical behavior for a superconducting material, the hysteresis loop for the LSMO/YBCO film reveals a change in shape due to the presence of a ferromagnetic moment. Here, the ferromagnetic behavior appears to be superimposed over the large Meissner effect of the superconducting layer.

The hysteresis loops in the out-of-plane direction are shown in Fig. 4(b). The behavior of the YBCO film is almost similar to that in the in-plane magnetization case with a slightly reduced moment. The data for both samples exhibit no change in the shape of the hysteresis loop, although the magnetization for the bilayer film is an order of magnitude smaller than that of the pristine YBCO film. This is verified by plotting the rescaled LSMO/YBCO data by 10 times (dashed line) in the figure. It appears that the magnetic moment of the LSMO layer compensates the diamagnetism significantly, resulting in a smaller overall magnetization value. These results suggest that the spins of the electrons in the superconducting phase may be aligned in the out-of-plane direction, which facilitates formation of out-of-plane vortices.

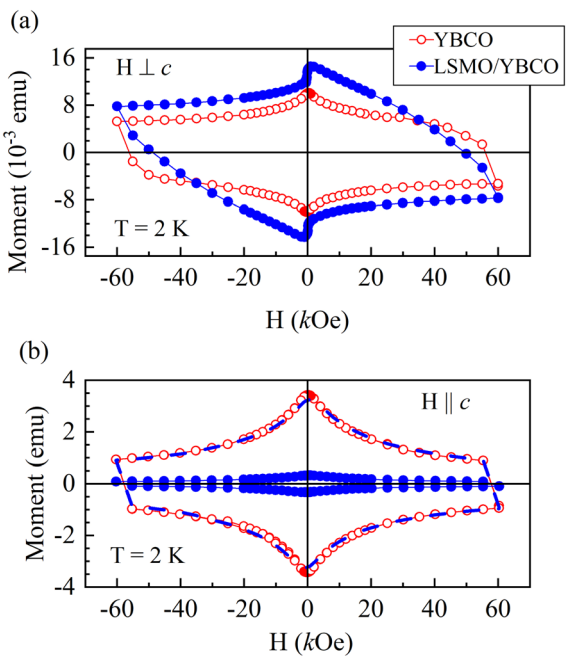

Fig. 4 Magnetization loops of the YBCO (open circles) and YBCO/LSMO (closed circles) films for the field (a) $\perp c$-axis and (b) $\|c$-axis at 2 K. The dashed line in (b) represents the LSMO/YBCO data multiplied by 10.

Transfer of holes has been observed between the cuprates and manganites using optical far-infrared spectroscopy. In $La_{0.67}Ca_{0.33}MnO_3$ (LCMO)/YBCO superlattices, polarized neutron reflectometry studies show suppression of magnetization at the LCMO and YBCO interface. In addition to this, the transformation of a few layers of ferromagnetic manganite into an antiferromagnetic state due to the hole charge transfer is also shown using the neutron reflectometry experiment.[35] Evidently, the behavior of the bilayer film observed here can be strongly influenced by the charge transfer across the interface, leading to a larger doped regime close to the interface.

In order to study this scenario further, we studied the Ba 4d and Y 3d core-level spectra using XPS. These elements essentially form the building blocks of the structure and provide little contribution to the valence and conduction bands, and are often called spectator elements. The photoemission final state effect for the core-level photoexcitation often manifests the changes in the electronic structure and hence provides a good way to study the signature of charge transfer across the interface without involving much complexity.[36] Ba 4d data collected from the YBCO and LSMO/YBCO samples are shown in Fig. 5. While Ba 4d photoemission is expected to show two spin–orbit split features, we observed three distinct peaks – none of them show an appropriate branching ratio, indicating the presence of multiple Ba 4d signals. The spectra from the YBCO sample are shown in Fig. 5(a). With a change in the photoemission geometry from normal emission (NE) to 25°-angled emission with respect to surface normal, the intensity of the peak at 86.4 eV binding energy reduces significantly with respect to the other features. The escape depth of the photoelectrons is sensitive to the emission angle; the 25°-angled emission will be slightly more surface sensitive than the normal emission case.[37–41] The change in intensity with the change in surface sensitivity suggests that the peak at 86.4 eV binding energy arises from bulk Ba sites while the features at higher binding energies are surface Ba contributions. This description is consistent with earlier studies of bulk single crystals.[42] In order to find the signatures of the surface and bulk peaks in the spectral function, we simulated the experimental spectra using a set of asymmetric Voigt functions representing the spin–orbit split features with the intensity ratio based on the degeneracy of the features. The simulated data are shown in Fig. 5(b) and (c) for the NE and 25° cases, respectively, excellently capturing the experimental spectral function. From this analysis, it is clear that the bulk and surface Ba $4d_{5/2}$ signals appear at 86.4 eV and 88.6 eV binding energies and the spin–orbit splitting is found to be 2.8 eV. The binding energy of the bulk Ba atoms is similar to the observation in the bulk single crystals of $YBa_2Cu_3O_7$.[42] The binding energy of the surface Ba atoms is similar to the divalent Ba in BaO.[43] While Ba is close to divalent in YBCO crystals, the

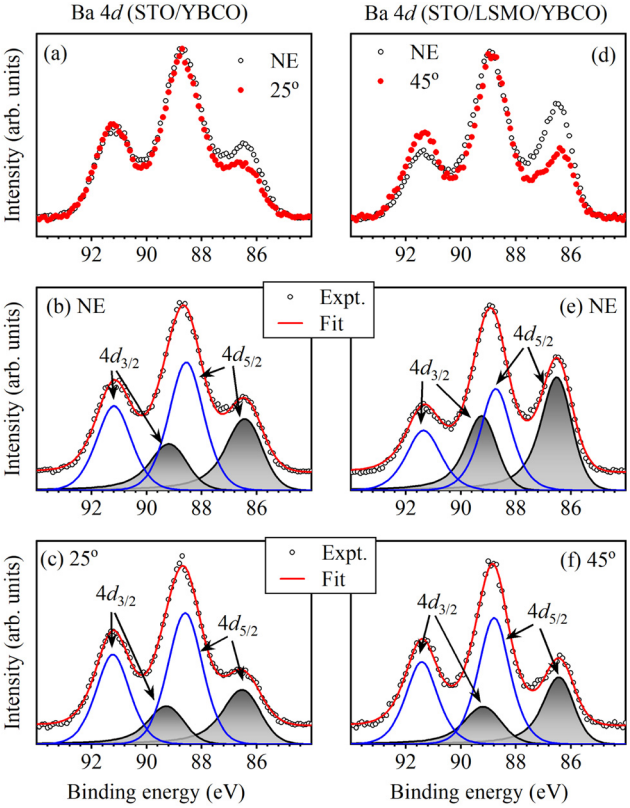

Fig. 5 Ba 4d spectra: (a) data for the YBCO film at normal emission (open circles) and 25°-angled emission (closed circles). Simulated spectra for (b) normal emission and (c) 25°-angled emission data; component peaks are shown in the bottom panel. (d) Data for the LSMO/YBCO film at normal emission (open circles) and 45°-angled emission (closed circles). Simulated spectra for (e) normal emission and (f) 45°-angled emission data; component peaks are shown in the bottom panel.

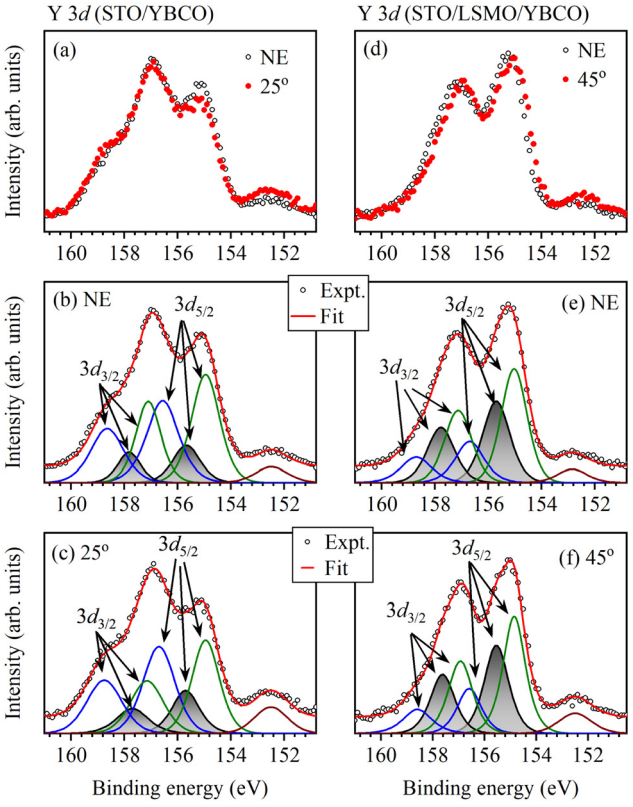

Fig. 6 Y 3d spectra: (a) data for the YBCO film at normal emission (open circles) and 25°-angled emission (closed circles). Simulated spectra for (b) normal emission and (c) 25°-angled emission data; component peaks are shown in the bottom panel. (d) Data for the LSMO/YBCO film at normal emission (open circles) and 45°-angled emission (closed circles). Simulated spectra for (e) the normal emission and (f) 45°-angled emission data; component peaks are shown in the bottom panel.

surface Ba atoms appear to be essentially divalent and the bulk Ba has some covalency as expected in solid systems.

The spectra from LSMO/YBCO are shown in Fig. 5(d) for the NE and 45°-angled emission cases exhibiting three distinct features similar to the YBCO case. Interestingly, the bulk feature in the bilayer data is significantly more intense than that in the YBCO case. This is curious considering the fact that the XPS data essentially represent the photoemission signal from the top few layers of the YBCO film as the escape depth of the Ba 4d photoelectrons will be about 20 Å.[37] The spectral change suggests a significant change in the electronic structure due to the presence of the LSMO layer below the YBCO layer.

In Fig. 6, we have shown the Y 3d spectra collected at different emission angles. The spectra from the YBCO sample shown in Fig. 6(a) exhibit 4 distinct features at 152.5, 155, 157 and 158.8 eV binding energies. This is unusual considering the photoemission studies in bulk YBCO crystals,[42,44] where Y 3d spectra often exhibit a two-peak structure for the spin–orbit split features. We notice that a change in the emission angle to 25° leads to a reduction in intensity at around 155 eV. The feature at 152.5 eV may be an impurity feature and becomes stronger in the 25°-angled emission case. We have simulated the experimental spectra considering peaks representing spin–orbit split Y 3d features; it was necessary to consider at least three sets of such features to satisfy the intensity ratio of the features to their degeneracy. The simulated spectra and the constituent peaks are shown in Fig. 6(b) and (c) for the NE and 25° emission cases, respectively. Y $3d_{5/2}$ features in each set appear at 155 eV, 155.7 eV and 156.6 eV. The spin–orbit splitting is found to be about 2.2 eV, which is similar to the earlier observations.[42,44] The peak at 156.6 eV may be attributed to the trivalent surface yttrium, while the one at 155.7 eV is an intermediate one and the peak at 155 eV is attributed to the bulk Y.[45]

In Fig. 6(d), we have shown the Y 3d spectra collected from the LSMO/YBCO sample exhibiting a slightly different scenario. With a change in the emission angle to 45°, the peaks appear to shift towards lower binding energy in contrast to the case for Ba photoemission. It turns out that these spectral functions can be simulated with three sets of peaks exhibiting similar peak positions for the constituent peaks as found in the YBCO sample, while their relative intensities are very different. The intensity of the bulk Y peak becomes dominant in the LSMO/YBCO sample, as also observed in the case of Ba

photoemission. The surface Y peak is significantly less intense in this case.

The overall reduction of intensity of the higher binding energy features in Ba 4d and Y 3d spectra in the LSMO/YBCO sample suggests that the positive valency at these sites is being compensated for due to additional electrons near the surface area in the LSMO/YBCO sample, making them comparable to the bulk spectra. Such a scenario is possible if there is a hole transfer across the interface to the LSMO layer. This is consistent with the magnetization data as conjectured above in the text and predicted in other systems as well.[46,47] Thus, the electron density in the YBCO layer will be enhanced, and will propagate to the surface of the sample.

4. Conclusion

In conclusion, we have grown high-quality thin films of $SrTiO_3/YBa_2Cu_3O_7$ and $SrTiO_3/La_{0.67}Sr_{0.33}MnO_3/YBa_2Cu_3O_7$ using a home-built ultra-high vacuum pulsed laser deposition system. The growth is found to be single crystalline, epitaxial and along the (001) direction. The in-plane and out-of-plane lattice parameters of the YBCO layer matches well with those of the bulk orthorhombic YBCO sample. The Curie temperature of the bilayer film is significantly smaller than the Curie temperature of bulk LSMO, suggesting a change in the electronic structure of the material in the bilayer. The easy axis of the magnetic moment lies along the in-plane direction of the film, while in the out-of-plane direction, diamagnetism dominates. Unidirectional anisotropy grows with cooling and becomes large in the superconducting phase.

The pristine YBCO film on the STO substrate exhibits superconductivity with strong diamagnetic behavior below 86 K for the magnetic field perpendicular to the surface. The measurements for the in-plane magnetic field exhibit the onset of transition at a slightly higher temperature. Interestingly, the LSMO/YBCO sample also shows diamagnetic behavior, a signature of superconductivity suggesting the coexistence of ferromagnetic order and superconductivity; the onset temperature of diamagnetism remains similar to that in the pristine case despite the presence of the ferromagnetic layer underneath. These results suggest this system to be a good case for the on-demand tuning of properties without significant effect on superconductivity.

Ba and Y core-level spectra reveal the signatures of different surface and bulk electronic structures. The intensity of the surface features reduces significantly in the LSMO/YBCO sample, indicating an overall enhancement of electron density near the surface area due to the transfer of holes from the YBCO to LSMO layers that also reduced the magnetic transition temperature as found in the magnetization data. A complex interplay of the Meissner effect and ferromagnetic moment has been observed, giving the plateau-like feature at higher applied magnetic fields. These results reveal an interesting platform of coexisting ferromagnetic order and superconductivity to realize exotic science and advanced technology.

Author contributions

Ankita Singh: conceptualization, methodology, data curation and analysis, and writing – original draft. Sawani Datta: data analysis. Ram Prakash Pandeya: methodology. Srinivas C. Kandukuri: methodology. Rudheer Bapat and Jayesh Parmar: HRTEM study. Kalobaran Maiti: conceptualization, methodology, data curation and analysis, writing – original draft, funding, all resources, and overall supervision.

Conflicts of interest

There are no conflicts to declare.

Acknowledgements

The authors acknowledge the financial support from the Department of Atomic Energy (DAE), Govt. of India (Project Identification no. RTI4003, DAE OM no. 1303/2/2019/R&D-II/DAE/2079 dated 11.02.2020). K. M. acknowledges financial supports from BRNS, DAE, Govt. of India under the DAE-SRC-OI Award (grant no. 21/08/2015-BRNS/10977) and J. C. Bose Fellowship (SB/S2/JCB-24/2014), DST, Govt. of India.

References

1 N. Kurita, M. Kimata, K. Kodama, A. Harada, M. Tomita, H. S. Suzuki, T. Matsumoto, K. Murata, S. Uji and T. Terashima, *Phys. Rev. B: Condens. Matter Mater. Phys.*, 2011, **83**, 214513.
2 G. Adhikary, N. Sahadev, D. Biswas, R. Bindu, N. Kumar, A. Thamizhavel, S. K. Dhar and K. Maiti, *J. Phys.: Condens. Matter*, 2013, **25**, 225701.
3 F. S. Bergeret, A. F. Volkov and K. B. Efetov, *Phys. Rev. Lett.*, 2001, **86**, 4096.
4 J. Hoppler, J. Stahn, Ch. Niedermayer, V. K. Malik, H. Bouyanfif, A. J. Drew, M. Rössle, A. Buzdin, G. Cristiani, H.-U. Habermeier, B. Keimer and C. Bernhard, *Nat. Mater.*, 2009, **8**, 315.
5 Z. Sefrioui, D. Arias, V. Pena, J. E. Villegas, M. Varela, P. Prieto, C. Leon, J. L. Martinez and J. Santamaria, *Phys. Rev. B: Condens. Matter Mater. Phys.*, 2003, **67**, 214511.
6 M. Djupmyr, S. Soltan, H.-U. Habermeier and J. Albrecht, *Phys. Rev. B: Condens. Matter Mater. Phys.*, 2009, **80**, 184507.
7 S. Soltan, J. Albrecht and H.-U. Habermeier, *Phys. Rev. B: Condens. Matter Mater. Phys.*, 2004, **70**, 144517.
8 M. J. Zhang, Y. W. Yin, T. S. Su, M. L. Teng, D. L. Zhang, X. G. Li and L. J. Zou, *Appl. Phys. Lett.*, 2013, **103**, 193506.
9 S. Chaudhuri, Y.-S. Chen and J. G. Lin, *ACS Omega*, 2023, **8**, 16694.
10 J. J. Wisser and Y. Suzuki, *AIP Adv.*, 2021, **11**, 015007.
11 C. Z. Chen, C. B. Cai, L. Peng, B. Gao, F. Fan, Z. Y. Liu, Y. M. Lu, R. Zeng and S. X. Dou, *J. Appl. Phys.*, 2009, **106**, 093902.

12 M. Houzet and A. I. Buzdin, *Phys. Rev. B: Condens. Matter Mater. Phys.*, 2006, **74**, 214507.
13 D. Samal and P. S. Anil Kumar, *J. Appl. Phys.*, 2011, **109**, 07E129.
14 R. S. Keizer, S. T. B. Gönnenwein, T. M. Klapwijk, G. Miao, G. Xiao and A. Gupta, *Nature*, 2006, **439**, 825.
15 H. Bhatt, Y. Kumar, C. L. Prajapat, C. J. Kinane, A. Caruana, S. Langridge, S. Basu and S. Singh, *ACS Appl. Mater. Interfaces*, 2022, **14**, 8565.
16 H.-Y. Wu, T. Zou, Z.-H. Cheng and Y. Sun, *Chin. Phys. Lett.*, 2009, **26**, 017502.
17 P. Przyslupski, I. Komissarov, W. Paszkowicz, P. Dluzewski, R. Minikayev and M. Sawicki, *Phys. Rev. B: Condens. Matter Mater. Phys.*, 2004, **69**, 134428.
18 P. Przyslupski, A. Tsarou, P. Dluzewski, W. Paszkowicz, R. Minikayev, K. Dybko, M. Sawicki, B. Dabrowski and C. Kimaball, *Supercond. Sci. Technol.*, 2006, **19**, 538.
19 J. Hemberger, A. Krimmel, T. Kurz, H.-A. Krug von Nidda, V. Yu. Ivanov, A. A. Mukhin, A. M. Balbashov and A. Loidl, *Phys. Rev. B: Condens. Matter Mater. Phys.*, 2002, **66**, 094410.
20 R. Bindu, G. Adhikary, S. K. Pandey, S. Patil and K. Maiti, *New J. Phys.*, 2010, **12**, 033026.
21 R. Bindu, G. Adhikary and K. Maiti, *J. Phys.: Conf. Ser.*, 2011, **273**, 012140.
22 R. Bindu, G. Adhikary, N. Sahadev, N. P. Lalla and K. Maiti, *Phys. Rev. B: Condens. Matter Mater. Phys.*, 2011, **84**, 052407.
23 J. D. Jorgensen, B. W. Veal, A. P. Paulikas, L. J. Nowicki, G. W. Crabtree, H. Claus and W. K. Kwok, *Phys. Rev. B: Condens. Matter Mater. Phys.*, 1990, **41**, 1863.
24 K.-R. Jeon, C. Ciccarelli, A. J. Ferguson, H. Kurebayashi, L. F. Cohen, X. Montiel, M. Eschrig, J. W. A. Robinson and M. G. Blamire, *Nat. Mater.*, 2018, **17**, 499.
25 M. Lorenz, H. Hochmuth, D. Matusch, M. Kusunoki, V. L. Svetchnikov, V. Riede, I. Stanca, G. Kastner and D. Hesse, *IEEE Trans. Appl. Supercond.*, 2001, **11**, 3209.
26 A. Singh, R. P. Pandeya, S. Dutta, S. C. Kandukuri and K. Maiti, *SciPost Phys. Proc.*, 2023, **11**, 007.
27 C.-H. Chen, A. Saiki, N. Wakiya, K. Shinozaki and N. Mizutani, *J. Cryst. Growth*, 2000, **219**, 253.
28 B. Liu, R. Zhang, Z. L. Xie, H. Lu, Q. J. Liu, Z. Zhang, Y. Li, X. Q. Xiu, P. Chen, P. Han, S. L. Gu, Y. Shi, Y. D. Zheng and W. J. Schaff, *J. Appl. Phys.*, 2008, **103**, 023504.
29 E. Dagotto, T. Hotta and A. Moreo, *Phys. Rep.*, 2001, **344**, 1153.
30 B. Náfrádi, P. Szirmai, M. Spina, A. Pisoni, X. Mettan, N. M. Nemes, L. Forró and E. Horváth, *Proc. Natl. Acad. Sci. U. S. A.*, 2020, **117**, 6417.
31 S. Jain, H. Sharma, A. K. Shukla, C. V. Tomy, V. R. Palkar and A. Tulapurkar, *Phys. B*, 2014, **448**, 103.
32 K. Maiti, *Europhys. Lett.*, 2008, **82**, 67006.
33 K. Maiti, V. R. R. Medicherla, S. Patil and R. S. Singh, *Phys. Rev. Lett.*, 2007, **99**, 266401.
34 S. M. Kumawat, G. D. Dwivedi, P. F. Su, W. S. Shyu, Y. H. Chien, P. W. Su, C. M. Chung, N. D. B. Fernandez, S. J. Sun, C.-H. Hsu, S. Yang and H. Chou, *J. Phys. Chem. C*, 2023, **127**, 6861.
35 M. A. Uribe-Laverde, D. K. Satapathy, I. Marozau, V. K. Malik, S. Das, K. Sen, J. Stahn, A. Ruhm, J.-H. Kim, T. Keller, A. Devishvili, B. P. Toperverg and C. Bernhard, *Phys. Rev. B: Condens. Matter Mater. Phys.*, 2013, **87**, 115105.
36 R. S. Singh and K. Maiti, *Phys. Rev. B: Condens. Matter Mater. Phys.*, 2007, **76**, 085102.
37 M. P. Seah and W. A. Dench, *Surf. Interface Anal.*, 1979, **1**, 2.
38 K. Maiti, P. Mahadevan and D. D. Sarma, *Phys. Rev. Lett.*, 1998, **80**, 2885.
39 K. Maiti, U. Manju, S. Ray, P. Mahadevan, I. H. Inoue, C. Carbone and D. D. Sarma, *Phys. Rev. B: Condens. Matter Mater. Phys.*, 2006, **73**, 052508.
40 A. Pramanik, R. P. Pandeya, K. Ali, B. Joshi, I. Sarkar, P. Moras, P. M. Sheverdyaeva, A. K. Kundu, C. Carbone, A. Thamizhavel, S. Ramakrishnan and K. Maiti, *Phys. Rev. B*, 2020, **101**, 035426.
41 R. P. Pandeya, A. P. Sakhya, S. Datta, T. Saha, G. De Ninno, R. Mondal, C. Schlueter, A. Gloskovskii, P. Moras, M. Jugovac, C. Carbone, A. Thamizhavel and K. Maiti, *Phys. Rev. B*, 2021, **104**, 094508.
42 K. Maiti, J. Fink, S. de Jong, M. Gorgoi, C. Lin, M. Raichle, V. Hinkov, M. Lambacher, A. Erb and M. S. Golden, *Phys. Rev. B: Condens. Matter Mater. Phys.*, 2009, **80**, 165132.
43 O. Karslioğlu, L. Trotochaud, I. Zegkinoglou and H. Bluhm, *J. Electron Spectrosc. Relat. Phenom.*, 2018, **225**, 55.
44 C. R. Brundle and D. E. Fowler, *Surf. Sci. Rep.*, 1993, **19**, 143.
45 D. Barreca, G. A. Battiston, D. Berto, R. Gerbasi and E. Tondello, *Surf. Sci. Spectra*, 2001, **8**, 234.
46 N. Nakagawa, H. Y. Hwang and D. A. Muller, *Nat. Mater.*, 2006, **5**, 204.
47 S. Mukherjee, B. Pal, D. Choudhury, I. Sarkar, W. Drube, M. Gorgoi, O. Karis, H. Takagi, J. Matsuno and D. D. Sarma, *Phys. Rev. B*, 2016, **93**, 245124.